Non-Gaussian diffusion near surfaces

Arthur Alexandre, Maxime Lavaud, Nicolas Fares, Elodie Millan, Yann Louyer, Thomas Salez, Yacine Amarouchene, Thomas Guérin, David S. Dean

Non-Gaussian diffusion near surfaces

Arthur Alexandre[a],[1] Maxime Lavaud[a],[1] Nicolas Fares,[1] Elodie Millan,[1] Yann Louyer,[1] Thomas Salez,[1,*] Yacine Amarouchene,[1,†] Thomas Guérin,[1,‡] and David S. Dean[1,2,§]

[1] *Univ. Bordeaux, CNRS, LOMA, UMR 5798, F-33400, Talence, France.*
[2] *Team MONC, INRIA Bordeaux Sud Ouest, CNRS UMR 5251, Bordeaux INP, Univ. Bordeaux, F-33400, Talence, France.*

We study the diffusion of particles confined close to a single wall and in double-wall planar channel geometries where the local diffusivities depend on the distance to the boundaries. Displacement parallel to the walls is Brownian as characterized by its variance, but it is non-Gaussian having a non-zero fourth cumulant. Establishing a link with Taylor dispersion, we calculate the fourth cumulant and the tails of the displacement distribution for general diffusivity tensors along with potentials generated by either the walls or externally, for instance gravity. Experimental and numerical studies of the motion of a colloid in the direction parallel to the wall give measured fourth cumulants which are correctly predicted by our theory. This system is a well-controlled physical realization of Brownian-yet-non-Gaussian diffusion generated by a fluctuating diffusivity mechanism for which the local diffusivity is quantified. These results provide additional tests and constraints for the inference of force maps and local transport properties near surfaces.

The transport properties of tracer particles in complex media can be very different from those observed in simple fluids. In the bulk of simple fluids, beyond molecular length and time scales, the motion of a colloidal particle satisfies two important properties: (i) its Mean Squared Displacement (MSD) increases linearly with time (diffusive behavior) and (ii) the probability distribution functions (PDF) of position increments are Gaussian. In complex media, exhibiting dynamical and spatial heterogeneities, or in presence of flows or active forces, both properties (i) and (ii) are generally not satisfied. Examples range from non-Gaussian transport in hydrodynamic flows, with consequences for chemical delivery in microfluidic environments [1], to experimental observations of *anomalous* diffusion in complex fluids and biological media [2–6] .

Tracer dynamics in a large class of complex media can be described as either *Fickian-yet-non-Gaussian*, *anomalous-yet-Brownian* or *Brownian-yet-Non-Gaussian Diffusion* (BNGD) [7–12]. These terms all refer to processes with linear-in-time MSDs but non-Gaussian PDFs. A generic explanation for this phenomenon is the *diffusing-diffusivity* mechanism Ref. [13]. In this scenario, BNGD is generated by a fluctuating diffusion constant, arising for example from fluctuations of the local density or of the gyration radius of complex macromolecules [14]. The diffusing-diffusivity mechanism has been further explored [15–23], but in most studies the assumptions invoked for the dynamically evolving diffusivity are generic but rather phenomenological. To the best of our knowledge, with the exception of the Brownian motion of an ellipsoidal particle [24–26], there is currently no experimental realization of a system exhibiting BNGD at all times where the local diffusivity is quantified both experimentally, numerically and theoretically over broad spatial and temporal ranges.

In this Letter, we study the BNGD of a tracer particle diffusing near a hard wall. In particular, we provide a calculation, that we verify experimentally and numerically, of the fourth cumulant of the displacement along the walls, which quantifies non-Gaussianity at all times. Hydrodynamic interactions at walls strongly modify the stochastic motion of neighboring objects [27–33]. The local diffusivity parallel to the wall depends on the distance to the wall which itself fluctuates due to diffusion perpendicular to the wall, thus generating the diffusing-diffusivity mechanism. Note that a similar situation was previously considered in Ref. [34], but that study mainly focused on the motion perpendicular to the wall: in this case, the non-Gaussian behavior due to diffusing diffusivity can be observed only at small times, since at long times the presence of an interaction potential with the wall induces non-Gaussian displacements – even for uniform diffusivity. Furthermore, the non-Gaussianity of the motion in the parallel direction could not be resolved in Ref [34]. Here, we focus on the motion parallel to the wall which is a genuine realization of diffusing diffusivity at all times. Our theoretical analysis identifies a formal link with Taylor dispersion. The characterization of the fourth cumulant is also important for the inference of force maps and local transport coefficients in heterogeneous environments [35, 36] and near surfaces [37].

Physical model. We consider a Brownian particle of radius a that is confined between two walls separated by a distance $2H_\mathrm{p}$, as shown in Fig. 1. The particle diffuses along the channel (*i.e.* the x-axis) and perpendicularly to it (*i.e.* the z-axis) with respective height-dependent diffusion coefficients $D_\parallel(z)$ and $D_\perp(z)$, and is subject to a potential $V(z)$. The probability density $p(z,t)$ about z at time t thus obeys the Fokker-Planck equation $\partial_t p =$

[a] These authors contributed equally to this work.

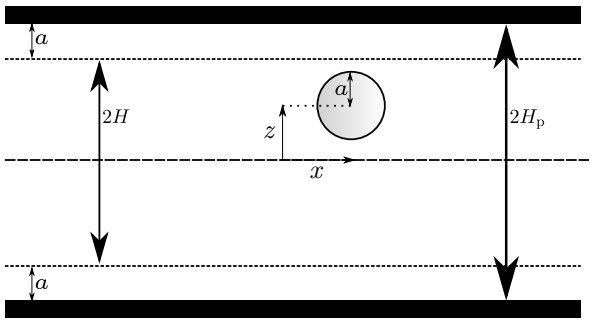

FIG. 1: Schematic: a particle of radius a diffuses in two dimensions, between two walls separated by a distance $2H_{\rm p}$.

$-\mathcal{H}p(z,t)$, where

$$\mathcal{H}\cdot = -\frac{\partial}{\partial z}\left\{D_\perp(z)\left[\frac{\partial}{\partial z}\cdot + \beta V'(z)\cdot\right]\right\} \ , \qquad (1)$$

with $\beta = 1/(k_{\rm B}T)$, where $k_{\rm B}$ is Boltzmann's constant and T the temperature. We assume no-flux conditions at the walls. In the long-time limit, the system equilibrates along the z direction and attains a Gibbs-Boltzmann distribution (see Fig. 2(a)):

$$p_0(z) = \frac{e^{-\beta V(z)}}{\int_{-H}^{H} e^{-\beta V(z')}dz'} \ . \qquad (2)$$

We denote by $Z_t \in [-H, H]$ the height of the center of the particle, $H = H_{\rm p} - a$ the effective channel height available to the particle, and X_t the position of the center of the particle along the channel. The second and fourth cumulants

$$\langle X_t^2\rangle_{\rm c} \equiv \langle X_t^2\rangle, \qquad \langle X_t^4\rangle_{\rm c} \equiv \langle X_t^4\rangle - 3\langle X_t^2\rangle^2 \ , \qquad (3)$$

characterize the transport properties of the particle. Here, $\langle\cdot\rangle$ denotes the ensemble average, and the initial condition is $X_{t=0} = 0$, while $Z_{t=0}$ follows the equilibrium distribution p_0. Note that $\langle X_t^4\rangle_{\rm c}$ vanishes if X_t is Gaussian, therefore its evaluation is the simplest way to quantify the non-Gaussian nature of the process X_t. We also define related non-Gaussianity parameter $\alpha(t) \equiv \langle X_t^4\rangle_{\rm c}/\langle X_t^2\rangle_{\rm c}^2$.

General theory. The process X_t obeys the stochastic differential equation:

$$dX_t = \sqrt{2D_\parallel(Z_t)}dB_{x,t} \ , \qquad (4)$$

where the Gaussian increments $dB_{x,t}$ have $\langle dB_{x,t}\rangle = 0$and $\langle dB_{x,t}^2\rangle = dt$. In Eq. (4), we use the Ito prescription of the stochastic calculus, however $D_\parallel(Z_t)$ is independent of X_t and so this choice is unimportant. Integrating Eq. (4) gives

$$X_t = \int_0^t \sqrt{2D_\parallel(Z_\tau)}dB_{x,\tau} \ . \qquad (5)$$

Squaring this and using the independence of $dB_{x,t}$ and Z_t, then taking the average yields

$$\langle X_t^2\rangle_{\rm c} \equiv \langle X_t^2\rangle = 2t\int_{-H}^{H} dz\, D_\parallel(z)p_0(z) = 2\left\langle D_\parallel\right\rangle_0 t \ , \qquad (6)$$

where $\langle\cdot\rangle_0$ denotes the average with respect to the equilibrium distribution $p_0(z)$. The MSD is purely linear in time, so that X_t is Brownian at all times.

Taking the fourth-power of Eq. (5) and using Wick's (or Isserli's) theorem [38] gives [39]

$$\frac{\langle X_t^4\rangle_{\rm c}}{12} = \int_0^t ds\int_0^t ds'[\langle D_\parallel(Z_s)D_\parallel(Z_{s'})\rangle - \langle D_\parallel\rangle_0^2]. \qquad (7)$$

Here, we draw an analogy with Taylor dispersion, for the dispersion of particles in channels in presence of hydrodynamic flows. We imagine the same process Z_t, but consider the convective displacement given along the channel by $Y_t = \int_0^t ds\ u(Z_s)$, where $u(z)$ is an arbitrary imposed flow field along the channel. The first two cumulants of Y_t in this problem are

$$\begin{aligned}\langle Y_t\rangle_{\rm c} &= \langle u\rangle_0 t,\\ \langle Y_t^2\rangle_{\rm c} &= \int_0^t ds\int_0^t ds'\ [\langle u(Z_s)u(Z_{s'})\rangle - \langle u\rangle_0^2].\end{aligned} \qquad (8)$$

Comparing the above expressions with Eqs. (6) and (7) we see that the second and fourth cumulants of X_t are proportional to the average and the variance of Y_t in a Taylor dispersion problem with the formal correspondance $u(z) = D_\parallel(z)$. Taylor dispersion has been widely studied [40–52], and we can exploit existing results for the MSD at all times from Ref. [52], yielding the explicit expression:

$$\begin{aligned}\langle X_t^4\rangle_{\rm c} = 24\int_{-H}^{H} dz\int_{-H}^{H} dz'\, D_\parallel(z)D_\parallel(z')p_0(z')\\ \times\sum_{\lambda>0}\left[\frac{t}{\lambda} - \frac{1-e^{-\lambda t}}{\lambda^2}\right]\psi_{{\rm R}\lambda}(z)\psi_{{\rm L}\lambda}(z') \ ,\end{aligned} \qquad (9)$$

where $\psi_{{\rm R}\lambda}(z)$ and $\psi_{{\rm L}\lambda}(z)$ respectively denote the right and left eigenfunctions of $\mathcal{H}$, with eigenvalue λ, and the normalization $\int_{-H}^{H} dz\ \psi_{{\rm L}\lambda}(z)\psi_{{\rm R}\lambda}(z) = 1$. In practice, this general expression can be evaluated by numerically computing the eigenfunctions after discretizing the operator $\mathcal{H}$. This formula simplifies at short times into (see SI [39]):

$$\left\langle X_t^4\right\rangle_{\rm c} \underset{t\to 0}{\simeq} 12\,t^2\left[\left\langle D_\parallel^2\right\rangle_0 - \left\langle D_\parallel\right\rangle_0^2\right] \ . \qquad (10)$$

We see that the initial non-Gaussianity parameter $\alpha(t = 0)$ is finite and is proportional to the variance of $D_\parallel(z)$ with respect to the equilibrium distribution, as in Ref. [13]. The late-time behavior is (see SI [39])

$$\langle X_t^4\rangle_{\rm c} \underset{t\to+\infty}{\simeq} 24\,(D_4 t - C_4) \ , \qquad (11)$$

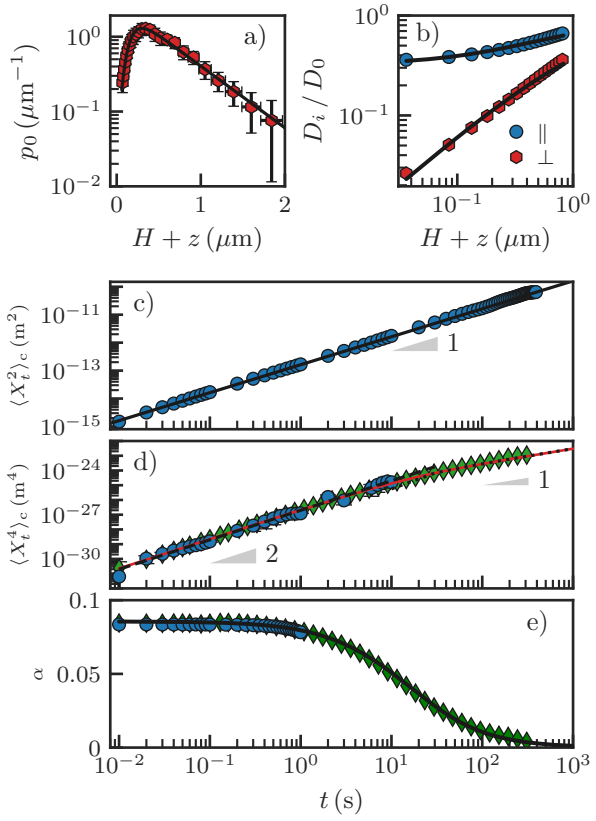

FIG. 2: (a) Experimentally-measured long-time PDF p_0 in position z, as a function of the distance $H+z$ to the bottom wall. The solid line represents the best fit to the Gibbs-Boltzmann distribution (2), using $V(z)$ defined in Eq. (16), with $B = 5.0$, $l_\mathrm{D} = 88$ nm and $l_\mathrm{B} = 526$ nm, and at room temperature. Here, $H_\mathrm{p} = 40$ μm. Error bars give 95% confidence intervals taking into account statistical error. (b) Experimentally-measured horizontal ($i = \parallel$) and vertical ($i = \perp$) local diffusion coefficients $D_i(z)$, normalized by the bulk value D_0. The solid lines represent the theoretical predictions $D_i(z)$ using Eqs. (17) and (18). (c) Experimentally-measured second cumulant $\langle X_t^2\rangle_\mathrm{c}$. The solid line corresponds to Eq. (6), with $\langle D_\parallel\rangle_0 = 0.58\,D_0$. The slope triangle indicates an exponent 1. (d) Experimentally-measured (blue dots) and numerically-simulated (green diamonds) fourth cumulant $\langle X_t^4\rangle_\mathrm{c}$. The solid line represents the theoretical expression of Eq. (9), while the dashed and dotted lines are the asymptotic expressions at short and long times, respectively, as given by Eqs. (10) and (11), with no adjustable parameter. The slope triangles indicate exponents 2 and 1. (e) Non-Gaussianity parameter $\alpha \equiv \langle X_t^4\rangle_\mathrm{c}/\langle X_t^2\rangle_\mathrm{c}^2$ as a function of time t, computed from the data in (c) and (d). Since it is constructed from a ratio between two quantities, the non-Gaussianity parameter is prone to larger errors than the fourth cumulant, thus the shorter accessible experimental temporal range.

where the explicit expression of C_4 is given in the Supplementary Information (SI) [39], and where:

$$D_4 = \left\langle \frac{\left[J(z)e^{\beta V(z)}\right]^2}{D_\perp(z)} \right\rangle_0 , \tag{12}$$

with:

$$J(z) = \int_{-H}^{z} dz' e^{-\beta V(z')} \left[D_\parallel(z') - \langle D_\parallel\rangle_0\right] . \tag{13}$$

From the above we see that the non-Gaussianity parameter satisfies $\alpha(t) \propto 1/t$, for large t.

Analytic strong confinement theory. We consider the case of a narrow channel where we approximate the local diffusion coefficients by the quadratic expressions [39, 53, 54]:

$$D_\perp(z) \approx D_{\perp 0}\left(1-\frac{z^2}{H^2}\right),\ D_\parallel(z) \approx D_{\parallel 0}\left(1-\frac{z^2}{H_\mathrm{s}^2}\right), \tag{14}$$

where H_s is a characteristic distance that can be considered as a slip-like length if $H_\mathrm{s} > H$. The coefficients $D_{\perp 0}$ and $D_{\parallel 0}$ depend on the effective channel height H and on the particle radius a. In principle, the no-slip boundary condition must impose that $D_\parallel(z)$ is zero at the walls, which would imply that $H_\mathrm{s} = H$. However, numerically, $D_\parallel(z)$ is found to be quadratic near the channel center and decays rapidly to zero near the walls [39, 54]. Here, Eq. (9) can be evaluated by noting that the eigenfunctions are the Legendre polynomials $P_n(z/H)$ of degree n, leading to

$$\frac{\langle X_t^4\rangle_\mathrm{c}}{24} = \frac{2D_{\parallel 0}^2 H^6 t}{135 D_{\perp 0} H_\mathrm{s}^4} - \frac{D_{\parallel 0}^2 H^8\left[1-e^{-\frac{6D_{\perp 0}t}{H^2}}\right]}{405 D_{\perp 0}^2 H_\mathrm{s}^4}. \tag{15}$$

In this model, there is only one relaxation time, equal to the time for the particle to diffuse perpendicularly. This result can be generalized to arbitrary $D_\parallel(z)$, keeping the same form of $D_\perp$, in which case many relaxation times appear (see SI [39]). The non-Gaussianity is such that $\alpha(0) = (12H^4)/(5(3H_\mathrm{s}^2 - H^2)^2)$ and is thus of order one. at short times, if one takes $H_\mathrm{s} = H$ then $\alpha(0) = 3/5$.

Experimental system. A polystyrene bead, with radius $a = 1.519 \pm 0.009$ μm diffuses in an aqueous NaCl solution confined between two glass walls. Its trajectory is tracked in three dimensions using Mie holography [37]. Here, $H_\mathrm{p} = 40$ μm, so that $H_\mathrm{p} \gg a$. The density mismatch of the particle is chosen such that the particle is visibly localized near the lower wall due to gravity (see Fig. 2(a)). So, the effect of the upper wall is negligible both in terms of hydrodynamic and conservative forces. The bead is submitted to a potential

$$\beta V(z) = B\,e^{-\frac{H+z}{l_\mathrm{D}}} + B\,e^{-\frac{H-z}{l_\mathrm{D}}} + \frac{z}{l_\mathrm{B}}. \tag{16}$$

The first two terms of the right-hand side are the screened electrostatic interactions between the negatively-charged

surfaces of the walls and the bead, as given mean-field theory [55], where $l_{\rm D}$ is the Debye length and B is a dimensionless number depending in particular on the wall and bead surface charges. We have used the superposition approximation, valid for gaps large compared to $l_{\rm D}$ so that the two potentials can be simply summed. The third term accounts for gravity: $l_{\rm B} = k_{\rm B}T/(\frac{4}{3}\pi a^3 \Delta\rho g)$ is the Boltzmann length, with g the gravitational acceleration, and $\Delta\rho$ the density mismatch between the polystyrene bead and the solution. Equations (2) and (16) are used to fit the experimentally measured equilibrium distribution $p_0(z)$. The agreement is good with $B = 5.0 \pm 0.3$, $l_{\rm D} = 88 \pm 2$ nm and $l_{\rm B} = 526 \pm 5$ nm, as shown in Fig. 2(a). Assuming a perfect sphere, the value of $l_{\rm B}$ gives a density mismatch $\Delta\rho = 53$ kg/m^3, which is within 5% error of the tabulated value of 50 kg/m^3.

Moving on to hydrodynamic interactions, $D_\parallel$ and $D_\perp$ are inferred from the experimentally observed trajectories [37, 39] and are shown in Fig. 2(b). The results agree with the Stokes-Einstein relations $D_i(z) = k_{\rm B}T/[6\pi a \mu_i(z)]$, where $i \in \{\parallel, \perp\}$ and where μ_i are the components of the effective viscosity tensor [56]. The transverse component reads [57]:

$$\mu_\parallel(z) = \mu_0 \left(1 - \frac{9}{16}\zeta + \frac{1}{8}\zeta^3 - \frac{45}{256}\zeta^4 - \frac{1}{16}\zeta^5\right)^{-1}, \quad (17)$$

with $\zeta = a/(z + H_{\rm p})$, and where μ_0 is the bulk viscosity. The normal component was derived in Ref. [56] as an infinite sum, which can be Padé-approximated to within 1% numerical accuracy by [58]

$$\mu_\perp(z) = \mu_0 \frac{6\,(z+H)^2 + 9a\,(z+H) + 2a^2}{6\,(z+H)^2 + 2a\,(z+H)} . \quad (18)$$

These expressions, through the associated diffusion coefficients, are in agreement with the experimental data at room temperature and with $\mu_0 = 1$ mPa.s for water, as shown in Fig. 2(b). Combined with the previously-mentioned equilibrium properties (see Eq. (16)), they can thus be used as inputs to compute the theoretical values of the fourth cumulant of X_t.

Comparison with theory. Experimentally, the displacements X_t are used to estimate $\langle X_t^2\rangle_{\rm c}$ and $\langle X_t^4\rangle_{\rm c}$, computed using the method of sliding averages described in SI [39] and leading to Figs. 2(c,d). First, the effective diffusion constant, $\langle D_\parallel\rangle_0$ defined in Eq. (6), is given numerically by $\langle D_\parallel\rangle_0 = 0.58\, D_0$, where $D_0 = k_{\rm B}T/(6\pi a\mu_0)$ is the bulk diffusion constant. This is in agreement with the experimental data shown in Fig. 2(c). Secondly, the short-time theoretical prediction in Eq. (10) correctly predicts the experimental data for $\langle X_t^4\rangle_{\rm c}$, with no adjustable parameter (see Fig. 2(d)). Lack of data at long times makes it difficult to check the late-time prediction given by Eq. (11). This result can however be verified through numerical simulations, as shown in Fig. 2(d), where the simulation details are given in SI [39]. The whole range of experimental and numerical data can be reproduced, up to error bars, by the exact prediction of Eq. (9), where the eigenfunctions and eigenvalues of $\mathcal{H}$ are computed numerically. Beyond validation of the theoretical predictions, our experiments thus confirm that the system studied is a physically realizable, and well-characterized example of BNGD.

Distribution of displacements. We now study the PDF $p(x,t)$ of the displacement x at time t, in order to determine in particular whether or not it displays apparent exponential tails, as often observed in BNGD [7, 8] and other contexts [59]. We consider a class of systems bounded in the z direction, with a single maximum in $D_{||}(z)$, as is the case in our simulations, experiments and the simple channel model. First, at short times, it is well known [13, 15, 24, 37] that

$$p(x,t) \simeq \int_{-H}^{H} dz\; p_0(z)\; \frac{e^{-x^2/[4D_\parallel(z)t]}}{\sqrt{4\pi D_\parallel(z) t}} . \quad (19)$$

An analysis of this expression shows that, for large x, one has $p(x,t) \propto e^{-x^2/4D_{||}(z^*)t}$, where z^* is the point where $D_{||}(z)$ is maximal. At larger times, the PDF can be analysed by calculating its moment-generating function $g(q,t) = \langle e^{qX_t}\rangle$, which reads:

$$g(q,t) = \left\langle e^{q\int_0^t dB_{x,s}\sqrt{2D_\parallel(Z_s)}}\right\rangle = \left\langle e^{q^2\int_0^t ds D_\parallel(Z_s)}\right\rangle , \quad (20)$$

where the last equality is obtained by averaging over the Gaussian noise $dB_{x,s}$. Interestingly, $g(q,t) = \langle e^{q^2 Y_t}\rangle$ is related to the moment-generating function for the above-mentioned Taylor dispersion problem. We can thus use the tools introduced in the context of Taylor dispersion [60–62] to obtain the extreme tails of $p(x,t)$ at long times (see SI [39]), with $p(x,t) \sim e^{-tf(x/t)}$. By extreme tails, we mean that $\xi = x/t$ is $\mathcal{O}(1)$, thus far from the diffusive scaling limit at late times where $x/\sqrt{t}$ is $\mathcal{O}(1)$. In SI [39], we show that for large ξ,

$$f(\xi) = \frac{1}{4D_{||}(z^*)}\left[\xi + \mathrm{sgn}(\xi)\sqrt{\frac{|D''_{||}(z^*)|D_\perp(z^*)}{2}}\right]^2 . \quad (21)$$

The paths contributing to $f(\xi)$ in this regime stay close to the region of maximal diffusivity, but they are rare and are exponentially suppressed with respect to paths which scale diffusively. The presence of Gaussian tails is generic for the class of problems studied here, and the exponential tails seen in other diffusing-diffusivity models [13] are absent. The fact that $D_\parallel(z)$ has a maximal value is the main difference between our system and those considered in Ref. [13], where the diffusion constant is unbounded. In fact, it was already noted in Ref. [13] that the PDF tails are generally not strictly exponential, depending on the local diffusivity distribution. The Gaussian tails in

our system contrast with the case of Continuous Time Random Walks [63], or diffusion in disordered confined media [12], where exponentials tails are present.

For small ξ, we find that $f(\xi) = \frac{\xi^2}{4\langle D_{||}\rangle_0}$, which matches with the late-time behavior of the diffusive scaling regime. The late-time corrections to Gaussianity in the diffusive-scaling region are dominated by the fourth-order cumulant, which gives a correction to the PDF that decays as $\sim 1/t$ (see SI [39]). Finally, replacing $q = -ik$ in Eq. (20) gives the Fourier transform $\hat{p}(k,t) = \int_{-\infty}^{\infty} dx\ e^{-ikx} p(x,t)$. This can be computed numerically (see SI [39]). Taking the inverse Fourier transform gives a numerical evaluation of $p(x,t)$ in good agreement with the numerical and experimental PDFs (see Fig. S2 in SI [39]). We have also examined the case where the channel width is much smaller ($H_\mathrm{p} = 5.5\,\mu$m). Similar effects are seen, but the asymptotic regime of linear temporal growth of the fourth cumulant is attained much more quickly.

Conclusion. In this Letter, we have addressed a canonical physical realization of Brownian-yet-Non-Gaussian Diffusion based on confined colloids, at all times. We have established a mapping onto Taylor dispersion, where the diffusivity is formally replaced by a flow field. This analogy also enabled us to provide quantitative predictions for the diffusion along the channel, which agree with experimental and numerical data with no additional fitting parameter apart from the physical ones obtained independently in the experiments. We have also shown that the extreme value tails of the pdf are not exponential but modified Gaussian in this generic class of models. Finally, it is interesting to note that the effective diffusion constant along the channel only depends on the equilibrium properties of the process normal to the wall, and is otherwise independent of its dynamics. The fourth cumulant, however, does depend on the precise details of the dynamics via the appearance of two-point probability density functions. The fourth cumulant thus carries extra information on the dynamics, and, as such, appears to be a key statistical observable that can further contribute to improve the experimental resolution for the inference of force maps and local transport properties near surfaces.

Acknowledgments

The authors thank Joshua McGraw and Maxence Arutkin for interesting discussions. They acknowledge financial support from the European Union through the European Research Council under EMetBrown (ERC-CoG-101039103) grant. Views and opinions expressed are however those of the authors only and do not necessarily reflect those of the European Union or the European Research Council. Neither the European Union nor the granting authority can be held responsible for them. The authors also acknowledge financial support from the Agence Nationale de la Recherche under EMetBrown (ANR-21-ERCC-0010-01), Softer (ANR-21-CE06-0029), Fricolas (ANR-21-CE06-0039), and ComplexEncounters (ANR-21-CE30-0020) grants. Finally, they thank the Soft Matter Collaborative Research Unit, Frontier Research Center for Advanced Material and Life Science, Faculty of Advanced Life Science at Hokkaido University, Sapporo, Japan.

* A.A. and M.L. contributed equally to this work.

* Electronic address: thomas.salez@cnrs.fr
† Electronic address: yacine.amarouchene@u-bordeaux.fr
‡ Electronic address: thomas.guerin@u-bordeaux.fr
§ Electronic address: david.dean@u-bordeaux.fr

[1] Aminian, M., Bernardi, F., Camassa, R., Harris, D. M. & McLaughlin, R. M. How boundaries shape chemical delivery in microfluidics. *Science* **354**, 0532 (2016).
[2] Bressloff, P. C. & Newby, J. M. Stochastic models of intracellular transport. *Rev. Mod. Phys.* **85**, 135 (2013).
[3] Höfling, F. & Franosch, T. Anomalous transport in the crowded world of biological cells. *Rep. Progr. Phys.* **76**, 046602 (2013).
[4] Ernst, D., Hellmann, M., Köhler, J. & Weiss, M. Fractional brownian motion in crowded fluids. *Soft Matt.* **8**, 4886–4889 (2012).
[5] Tolić-Nørrelykke, I. M., Munteanu, E.-L., Thon, G., Oddershede, L. & Berg-Sørensen, K. Anomalous diffusion in living yeast cells. *Phys. Rev. Lett.* **93**, 078102 (2004).
[6] Shen, H. *et al.* Single particle tracking: from theory to biophysical applications. *Chemical reviews* **117**, 7331–7376 (2017).
[7] Wang, B., Anthony, S. M., Bae, S. C. & Granick, S. Anomalous yet brownian. *Proc. Nat. Acad. Sc.* **106**, 15160–15164 (2009).
[8] Wang, B., Kuo, J., Bae, S. C. & Granick, S. When brownian diffusion is not gaussian. *Nature materials* **11**, 481–485 (2012).
[9] Skaug, M. J., Mabry, J. & Schwartz, D. K. Intermittent molecular hopping at the solid-liquid interface. *Phys. Rev. Lett.* **110**, 256101 (2013).
[10] Leptos, K. C., Guasto, J. S., Gollub, J. P., Pesci, A. I. & Goldstein, R. E. Dynamics of enhanced tracer diffusion in suspensions of swimming eukaryotic microorganisms. *Phys. Rev. Lett.* **103**, 198103 (2009).
[11] Guan, J., Wang, B. & Granick, S. Even hard-sphere colloidal suspensions display fickian yet non-gaussian diffusion. *ACS nano* **8**, 3331–3336 (2014).
[12] Chakraborty, I. & Roichman, Y. Disorder-induced fickian, yet non-gaussian diffusion in heterogeneous media. *Phys. Rev. Res.* **2**, 022020 (2020).
[13] Chubynsky, M. V. & Slater, G. W. Diffusing diffusivity: A model for anomalous, yet brownian, diffusion. *Phys. Rev. Lett.* **113**, 098302 (2014).
[14] Yamamoto, E., Akimoto, T., Mitsutake, A. & Metzler, R. Universal relation between instantaneous diffusivity and radius of gyration of proteins in aqueous solution. *Phys. Rev. Lett.* **126**, 128101 (2021).

[15] Chechkin, A. V., Seno, F., Metzler, R. & Sokolov, I. M. Brownian yet non-gaussian diffusion: from superstatistics to subordination of diffusing diffusivities. *Phys. Rev. X* **7**, 021002 (2017).

[16] Sposini, V., Chechkin, A. & Metzler, R. First passage statistics for diffusing diffusivity. *J. Phys. A: Math Theor* **52**, 04LT01 (2018).

[17] Lanoiselée, Y., Moutal, N. & Grebenkov, D. S. Diffusion-limited reactions in dynamic heterogeneous media. *Nat. Comm.* **9**, 4398 (2018).

[18] Lanoiselée, Y. & Grebenkov, D. S. A model of non-gaussian diffusion in heterogeneous media. *J. Phys. A: Math. Theor.* **51**, 145602 (2018).

[19] Jain, R. & Sebastian, K. L. Diffusion in a crowded, rearranging environment. *J. Phys. Chem. B* **120**, 3988–3992 (2016).

[20] Jain, R. & Sebastian, K. L. Diffusing diffusivity: survival in a crowded rearranging and bounded domain. *J. Phys. Chem. B* **120**, 9215–9222 (2016).

[21] Yin, Q., Li, Y., Marchesoni, F., Nayak, S. & Ghosh, P. K. Non-gaussian normal diffusion in low dimensional systems. *Frontiers of Physics* **16**, 1–14 (2021).

[22] Miotto, J. M., Pigolotti, S., Chechkin, A. V. & Roldán-Vargas, S. Length scales in brownian yet non-gaussian dynamics. *Phys. Rev. X* **11**, 031002 (2021).

[23] Hidalgo-Soria, M. & Barkai, E. Hitchhiker model for laplace diffusion processes. *Phys. Rev. E* **102**, 012109 (2020).

[24] Han, Y. *et al.* Brownian motion of an ellipsoid. *Science* **314**, 626–630 (2006).

[25] Munk, T., Höfling, F., Frey, E. & Franosch, T. Effective perrin theory for the anisotropic diffusion of a strongly hindered rod. *EPL (Europhysics Letters)* **85**, 30003 (2009).

[26] Czajka, P., Antosiewicz, J. M. & Długosz, M. Effects of hydrodynamic interactions on the near-surface diffusion of spheroidal molecules. *ACS omega* **4**, 17016–17030 (2019).

[27] Felderhof, B. Effect of the wall on the velocity autocorrelation function and long-time tail of brownian motion. *J. Phys. Chem. B* **109**, 21406–21412 (2005).

[28] Elgeti, J., Winkler, R. G. & Gompper, G. Physics of microswimmers—single particle motion and collective behavior: a review. *Rep. Progr. Phys.* **78**, 056601 (2015).

[29] Jeney, S., Lukić, B., Kraus, J. A., Franosch, T. & Forró, L. Anisotropic memory effects in confined colloidal diffusion. *Phys. Rev. Lett.* **100**, 240604 (2008).

[30] Huang, K. & Szlufarska, I. Effect of interfaces on the nearby brownian motion. *Nat. Comm.* **6**, 1–6 (2015).

[31] Choudhury, U., Straube, A. V., Fischer, P., Gibbs, J. G. & Höfling, F. Active colloidal propulsion over a crystalline surface. *New J. Phys.* **19**, 125010 (2017).

[32] Hertlein, C., Helden, L., Gambassi, A., Dietrich, S. & Bechinger, C. Direct measurement of critical casimir forces. *Nature* **451**, 172–175 (2008).

[33] Helden, L., Eichhorn, R. & Bechinger, C. Direct measurement of thermophoretic forces. *Soft Matt.* **11**, 2379–2386 (2015).

[34] Matse, M., Chubynsky, M. V. & Bechhoefer, J. Test of the diffusing-diffusivity mechanism using near-wall colloidal dynamics. *Phys. Rev. E* **96**, 042604 (2017).

[35] Serov, A. S. *et al.* Statistical tests for force inference in heterogeneous environments. *Scientific Reports* **10**, 1–12 (2020).

[36] Frishman, A. & Ronceray, P. Learning force fields from stochastic trajectories. *Phys. Rev. X* **10**, 021009 (2020).

[37] Lavaud, M., Salez, T., Louyer, Y. & Amarouchene, Y. Stochastic inference of surface-induced effects using brownian motion. *Phys. Rev. Res.* L032011 (2021). Publisher: APS.

[38] Coffey, W. & Kalmykov, Y. P. *The Langevin equation: with applications to stochastic problems in physics, chemistry and electrical engineering*, vol. 27 (World Scientific, 2012).

[39] See Supplemental Material at [URL will be inserted by publisher] for further experimental, numerical and analytical details, where we also cite Refs. [64–68].

[40] Barton, N. On the method of moments for solute dispersion. *J. Fluid. Mech.* **126**, 205–218 (1983).

[41] Biswas, R. R. & Sen, P. N. Taylor dispersion with absorbing boundaries: A stochastic approach. *Phys. Rev. Lett.* **98**, 164501 (2007).

[42] Vedel, S., Hovad, E. & Bruus, H. Time-dependent taylor–aris dispersion of an initial point concentration. *J. Fluid. Mech.* **752**, 107–122 (2014).

[43] Li, Z. *et al.* Near-wall nanovelocimetry based on total internal reflection fluorescence with continuous tracking. *Journal of Fluid Mechanics* **766**, 147–171 (2015).

[44] Guérin, T. & Dean, D. S. Force-induced dispersion in heterogeneous media. *Phys. Rev. Lett.* **115**, 020601 (2015).

[45] Guérin, T. & Dean, D. S. Kubo formulas for dispersion in heterogeneous periodic nonequilibrium systems. *Phys. Rev. E* **92**, 062103 (2015).

[46] Vilquin, A. *et al.* Time dependence of advection-diffusion coupling for nanoparticle ensembles. *Phys. Rev. Fluids* **6**, 064201 (2021).

[47] Brenner, H. & Edwards, D. A. *Macrotransport Processes* (Butterworth-Heinemann, 1993).

[48] Mercer, G. & Roberts, A. A complete model of shear dispersion in pipes. *Japan journal of industrial and applied mathematics* **11**, 499–521 (1994).

[49] Balakotaiah, V., Chang, H.-c. & Smith, F. Dispersion of chemical solutes in chromatographs and reactors. *Philosophical Transactions of the Royal Society of London. Series A: Physical and Engineering Sciences* **351**, 39–75 (1995).

[50] Marbach, S. & Alim, K. Active control of dispersion within a channel with flow and pulsating walls. *Phys. Rev. Fluids* **4**, 114202 (2019).

[51] Watt, S. D. & Roberts, A. J. The accurate dynamic modelling of contaminant dispersion in channels. *SIAM J. Appl. Math.* **55**, 1016–1038 (1995).

[52] Alexandre, A., Guérin, T. & Dean, D. S. Generalized Taylor dispersion for translationally invariant microfluidic systems. *Phys. Fluids* **33**, 082004 (2021).

[53] Lau, A. W. & Lubensky, T. C. State-dependent diffusion: Thermodynamic consistency and its path integral formulation. *Phys. Rev. E* **76**, 011123 (2007).

[54] Avni, Y., Komura, S. & Andelman, D. Brownian motion of a charged colloid in restricted confinement. *Phys. Rev. E* **103**, 042607 (2021).

[55] Israelachvili, J. N. *Intermolecular and surface forces, second edition* (Academic press, London, 1991).

[56] Brenner, H. The slow motion of a sphere through a viscous fluid towards a plane surface. *Chemical Engineering Science* **16**, 242–251 (1961).

[57] Faxen, H. Die bewegung einer starren kugel langs der achse eines mit zaher flussigkeit gefullten rohres. *Arkiv*

for Matemetik Astronomi och Fysik **17**, 1–28 (1923).

[58] Bevan, M. A. & Prieve, D. C. Hindered diffusion of colloidal particles very near to a wall: Revisited. *J. Chem. Phys.* **113**, 1228–1236 (2000).

[59] Silva, A. C., Prange, R. E. & Yakovenko, V. M. Exponential distribution of financial returns at mesoscopic time lags: a new stylized fact. *Physica A: Statistical Mechanics and its Applications* **344**, 227–235 (2004).

[60] Haynes, P. & Vanneste, J. Dispersion in the large-deviation regime. part 2. cellular flow at large péclet number. *J. Fluid Mech.* **745**, 351–377 (2014).

[61] Haynes, P. & Vanneste, J. Dispersion in the large-deviation regime. part 1: shear flows and periodic flows. *J. Fluid Mech.* **745**, 321–350 (2014).

[62] Kahlen, M., Engel, A. & Van den Broeck, C. Large deviations in taylor dispersion. *Phys. Rev. E* **95**, 012144 (2017).

[63] Barkai, E. & Burov, S. Packets of diffusing particles exhibit universal exponential tails. *Phys. Rev. Lett.* **124**, 060603 (2020).

[64] Gardiner, C. W. *Stochastic methods for physics, and handbook for the natural and social sciences* (Springer Series in Synergetics, 2009).

[65] Øksendal, B. *Stochastic differential equations* (Springer, New-York, 2003).

[66] Kurzthaler, C., Leitmann, S. & Franosch, T. Intermediate scattering function of an anisotropic active brownian particle. *Scientific reports* **6**, 1–11 (2016).

[67] Cramér, H. *Mathematical methods of statistics* (Princeton university press, 1946).

[68] Touchette, H. The large deviation approach to statistical mechanics. *Phys. Rep.* **478**, 1–69 (2009).